Oscillatory behavior of Rydberg-state total cross sections in the collisions Ne^+-He and He^+-Ne

B. Andresen
Chemistry Laboratory III, H. C. Ørsted Institute, Universitetsparken 5, DK-2100 Copenhagen Ø, Denmark

K. Jensen and E. Veje
Physics Laboratory II, H. C. Ørsted Institute, Universitetsparken 5, DK-2100 Copenhagen Ø, Denmark
(Received 7 October 1976)

The Ne^+-He and He^+-Ne collisions have been studied by means of optical spectrometry in the projectile energy range 10–150 keV. Very similar and regular oscillations in the Rydberg-state total cross sections are found for He I in both collisions and for singlet as well as triplet excitation. These oscillations are well described by the Rosenthal model. The He I $4d\,^{1,3}D$ states display two superimposed oscillations for center-of-mass collision energies above 6.4 keV. We interpret this as the opening of a third exit channel, believed to be the He I $4f\,^{1,3}F$. No (or very little) structure is found in the Rydberg-state total cross sections for He II, Ne I, Ne II, or Ne III levels.

I. INTRODUCTION

Oscillatory structure has been observed in total Rydberg-state excitation cross sections in several ion-atom collision systems. Recently Andersen *et al.*[1] investigated collisions between neon atoms and ions ranging from Li^+ to Al^+ experimentally with the purpose of finding general trends in the oscillatory behavior. References to earlier works may be found in that paper.

It is customary to explain oscillatory structure in the total excitation cross section in terms of the Rosenthal model.[2,3] This model, however, need not be a good *a priori* description for Rydberg-state excitation phenomena at projectile velocities $\gtrsim v_0$, the orbital velocity of the valence electrons. Therefore we felt it desirable to perform systematic experimental studies of oscillatory structure in Rydberg-state excitations up to such rather high velocities, and use these observations as a basis for conclusions *a posteriori* about the applicability of this excitation model.

We have earlier found structure in the Ne^+-He collision,[4] and since it is easy to study this collision together with its reverse, the He^+-Ne collision, we decided to investigate these two collisions further. Also, other investigators have spent much effort on $(HeNe)^+$, so a great deal is known about this system.[5,6] The recent studies of Hasselkamp *et al.*[7] in the projectile energy range 100–1000 keV and of Isler[8] below 9 keV supplement our intermediate energy range (10–150 keV) measurements well, although they have limited themselves to only a few states. A crucial basis for our interpretation of the experimental data is provided by the potential-energy-curve calculations of Sidis and Lefebvre-Brion[9] and of Blint.[10] Unfortunately they only include the lowest excited states, but from these good estimates can be made of the states pertaining to our experiments.

II. EXPERIMENTAL

Excitation functions, polarizations, and relative emission cross sections were measured for a large number of levels in the Ne^+-He and He^+-Ne collisions in the projectile energy range 10–150 keV. The accelerator has been described previously.[11] Two monochromators served as photon analyzers: a McPherson model 2051, $f/8.7$, working in the wavelength region 200–1200 nm, with an EMI 9659 QB photomultiplier, and a McPherson model 218, $f/5.3$, 200–600 nm, with an EMI 6256 SA photomultiplier. Both monochromators underwent quantum-efficiency calibration on relative scales by using an Optronic model 245 *C* lamp as well as a low-current carbon arc as standards of spectral irradiance in connection with a $BaSO_4$ screen. The calibrations obtained by using the two different standards of spectral irradiance agreed well with each other. The calibration procedure has been described together with the procedure for determining the instrumental polarization.[12] Procedures for data taking and reduction are given in Ref. 13. Branching ratios used to transform the He I emission cross sections into apparent excitation cross sections were calculated from the transition probabilities listed by Wiese *et al.*[14] The pressure was measured with a Baraton capacitance manometer, which made it easy to compare relative cross sections for excitation of the same level in the two collisions to a high degree of precision.

The relative He I cross sections reported here are on the same arbitrary scale, and they can be brought to an absolute one by comparison with the

absolute cross sections reported for the He^+-Ne collision by Muller and de Heer,[15] or for both collisions by Hasselkamp *et al.*[7]

III. RESULTS AND DISCUSSION

A. Rosenthal model

The Rosenthal model[2,3] assumes that two exit channels, 2 and 3 in Fig. 1, of the temporary molecular complex are coherently excited from the entrance channel 1, usually by curve crossings at A and B. When the states 2 and 3 mix at the point E, either through a third curve crossing or through term approach, the separated atom states will oscillate in intensity with the phase

$$\phi = \frac{1}{\hbar v}\int_{A,B}^{E}(E_3 - E_2)dR + \phi_0 \approx \frac{\Delta E\,\Delta R}{\hbar v} + \phi_0, \qquad (1)$$

and π out of phase due to the difference in phase picked up along AE and BE. v is an average velocity in the region A,B to E. Since the area ABE is almost independent of impact parameter, the oscillations will appear in the total cross sections as well as in the differential cross sections. When plotted versus v^{-1}, the peak order $N = \phi/2\pi$ is a linear function whose slope gives $\Delta E \Delta R$ and intercept ϕ_0. With a curve crossing at E, $\phi_0 = \frac{1}{4}\pi$ and the oscillation amplitude decreases for increasing v, whereas term approach predicts $\phi_0 = 0$ and constant oscillation amplitude.[3]

B. He I cross sections

It is generally found in the two collisions studied here, that the excitation cross sections for a HeI singlet level and the corresponding triplet term have the same structure as a function of the projectile velocity. This is exemplified in Figs. 2 and 3, where apparent excitation cross sections for the HeI $3s\,^{1,3}S$ and $4d\,^{1,3}D$ levels are plotted as a

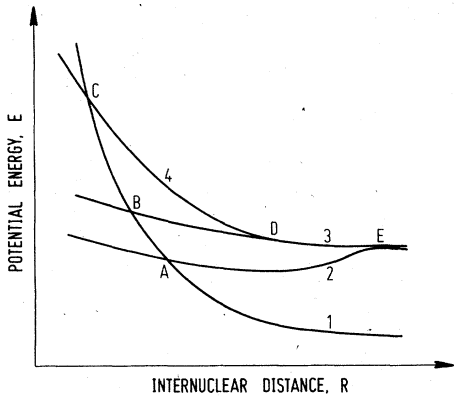

FIG. 1. Potential energy curves associated with Rosenthal oscillations.

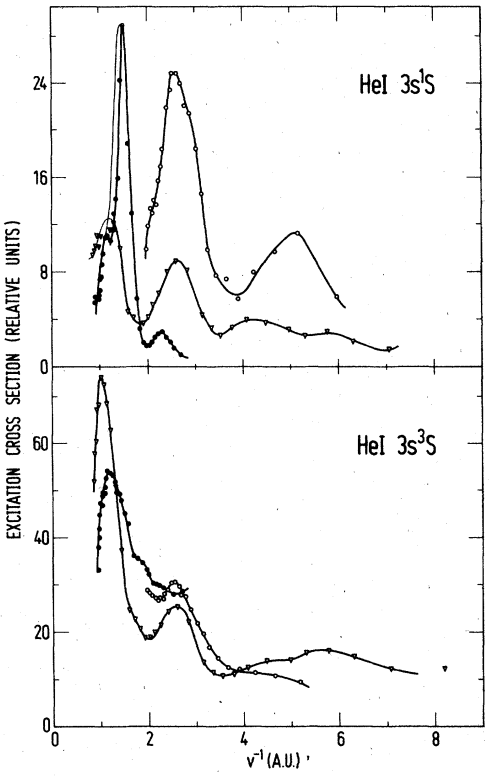

FIG. 2. Excitation cross sections for He I $3s\,^{1,3}S$. ●, He^+-Ne; ○, Ne^+-He; ▽, He^+-Ne, from Ref. 15.

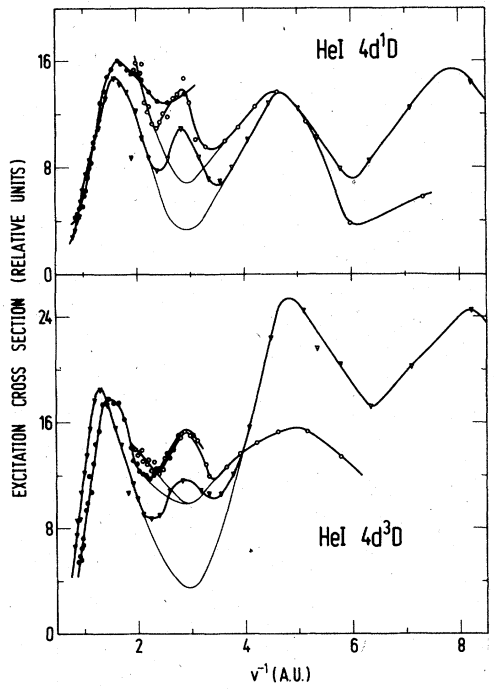

FIG. 3. Excitation cross sections for He I $4d\,^{1,3}D$. ●, He^+-Ne; ○, Ne^+-He; ▽, He^+-Ne, from Ref. 15.

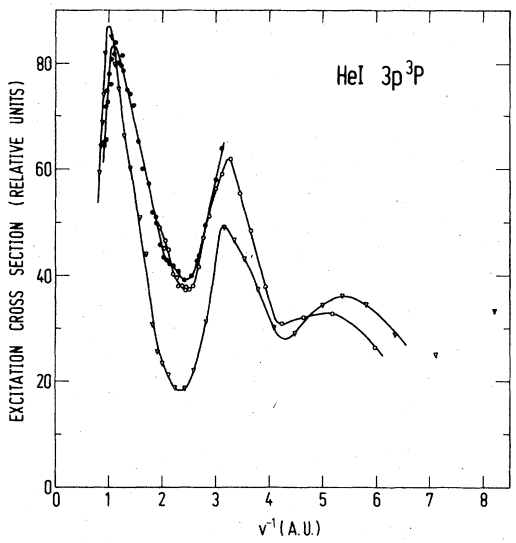

FIG. 4. Excitation cross sections for HeI $3p\,^3P$. ●, He^+-Ne; ○, Ne^+-He; ▽, He^+-Ne, from Ref. 15.

function of v^{-1} for the He^+-Ne and Ne^+-He collisions. Also shown are the He^+-Ne data of Muller and de Heer,[15] brought to the same arbitrary ordinate scale as ours. The agreement with their results is in all cases very good except at the lowest energies.

It may also be seen from Figs. 2 and 3, and especially Fig. 4 which contains the excitation cross section for the HeI $3p\,^3P$ level, that the cross section for exciting a HeI level in the He^+-Ne collision is close to the cross section for excitation in the reverse Ne^+-He collision. The same agreement has been observed by Hasselkamp *et al.*[7] at higher energies (100–1000 keV), but it differs from the behavior just above threshold (10 eV–1 keV) as measured by Tolk *et al.*,[6] who generally found much more pronounced structure in the He^+-Ne collision than in the Ne^+-He collision.

When the peak order N is plotted versus the inverse velocity, v^{-1} for the HeI $3s\,^{1,3}S$ and $3p\,^3P$ data (Figs. 2 and 4), we obtain a straight line as one would expect if the Rosenthal model describes the system well. A further check on the validity of the model could be obtained by measuring those NeI levels which would be expected to oscillate in intensity with the opposite phase of the reported HeI levels. Unfortunately we have been unable to measure any of these NeI lines, either because they were too weak, or because they were outside the wavelength region of our monochromator. However, the very regularly spaced oscillations in the HeI cross sections are sufficient indication that the Rosenthal model retains its applicability at these fairly high velocities. Table I gives the phase intercept ϕ_0 and interference area, $\Delta E\,\Delta R$ for the various HeI levels. The accuracy of the data (generally ±10%) makes it difficult to extrapolate to $v^{-1}=0$ and reliably distinguish between $\phi_0 = 0$ and $\frac{1}{4}\pi$; however the large oscillation amplitude for small v^{-1} indicates that the distant interaction in all cases is a term approach, not a curve crossing. With an average distance between the exit channels of 3 eV this interaction will then take place at an internuclear distance of ~15 Å.

If we accept the Rosenthal model, the two findings mentioned in the beginning of this section can be explained by reference to the calculated $(HeNe)^+$ potential curves of Fig. 5. The curves A and B are, respectively, the $Ne^+(2\,^2P^0)+He(1\,^1S)$ and $He^+(1\,^2S)+Ne(2\,^1S)$ entrance channels, and C, C' and

TABLE I. Phase intercept ϕ_0 and interference area $\Delta E\,\Delta R$ obtained by a least-squares fit to the peak orders in Figs. 2–4 and 7. "Slow" and "rapid" refer to the deconvolution of the slow and rapid oscillations in the cross sections of Figs. 3 and 7.

Level in HeI		$\phi_0/2\pi$ a	$\phi_0/2\pi$ b	$\Delta E\,\Delta R$ (eV Å) a	$\Delta E\,\Delta R$ (eV Å) b	Threshold (keV) a	Threshold (keV) b
$3s\,^1S$		−0.05	0.25	36	59	...	...
$3s\,^3S$		0.38	0.46	52	50	...	...
$3p\,^3P$		0.39	0.50	45	42	...	...
$3p\,^3P$	slow	0.73 [c]		1.4 [c]		...	
	rapid	−0.12 [c]		10.1 [c]		...	
$4d\,^1D$	slow	0.46	0.52	30	29	...	...
	rapid	−0.38	−0.13	74	65	6.1	6.1
$4d\,^3D$	slow	0.61	0.60	26	27	...	...
	rapid	−0.08	0.04	66	63	6.4	5.5

[a] Present data.
[b] Fit to data of Ref. 15.
[c] Fit to data of Ref. 6.

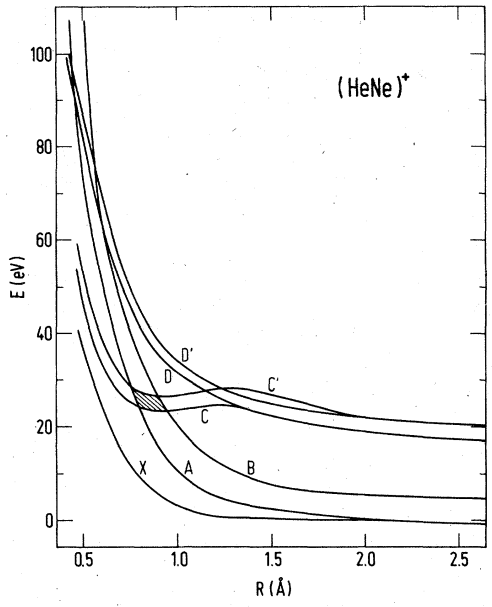

FIG. 5. $(HeNe)^+$ potential energy curves, from Ref. 9. X and A dissociate to $He(1\,^1S) + Ne^+(2\,^2P^0)$, B to $He^+(1\,^2S) + Ne(2\,^1S)$, C and D to $He^+(1\,^2S) + Ne(3P^0)$, C' and D' to $He(2S) + Ne^+(2\,^2P^0)$; C and C' are triplet states, D and D' singlets.

D, D' the triplet and singlet levels separating to $He^+ + Ne(3\,^{3,1}P^0)$, $Ne^+ + He(2\,^{3,1}S)$. Potential curves for the levels measured in this paper have not been calculated, but they presumably follow the shape of C, C' and D, D' at a slightly higher energy, so that semiquantitative conclusions can be based on the potentials in Fig. 5.

For triplet excitation the difference between the interference area ACC' for the Ne^+-He collision and that, BCC' for the He^+-Ne collision is the small shaded area $AC'BC$. Being only $\sim\frac{1}{2}$ eV Å it is much smaller than the total area of ~45 eV Å and therefore does not change the oscillation frequency noticeably, hence the good agreement between the He^+-Ne and Ne^+-He results at the same velocities. The small difference in ionization potential between He and Ne (3.02 eV) is easily adjusted for so that in both cases v is an average velocity over the interference distance. This explanation breaks down at energies close to threshold where strong interaction between the curve crossings at the four corners of $AC'BC$ together with an increased dependence of v on the impact parameter tend to make the phase difference, Eq. (1) vary with impact parameter and thus wash out the oscillations in the total cross section. The effect should be the stronger for the lower potential curve (A') in accord with experimental findings.[6]

The high degree of agreement between singlet and triplet scattering stems from the almost equal areas between the curves $A(B)DD'$ and $A(B)CC'$. Only at short internuclear distances do the distances among the singlet and triplet curves differ significantly, but that has a small effect on the total interference area.

The ratio between cross sections for excitation of a HeI triplet term and the corresponding singlet level is in the range 0.5–2, varying with projectile velocity as demonstrated in Fig. 6. The variations, however, do not coincide with the oscillations in the separate cross sections. The structure is generally more pronounced in the singlet cross section than it is in the triplet cross section as well as in cross sections for levels with low principal quantum number. The ratio should assume a value close to 3 for a sufficiently long-lived molecular complex where all past history of the electrons has been washed out. However, in a fast collision there may not be sufficient time for this equilibration. In addition the amplitude of a He triplet wave function in the vicinity of the nucleus (where the excitation takes place) is smaller than the amplitude of the corresponding singlet wave function. Both factors will reduce the ratio somewhat from 3.

We have also observed structure in HeI excitation cross sections for other ion-atom collisions, and since the general features of the potential curves in Fig. 5 will apply equally well for these, oscillatory structure will presumably occur for HeI levels in several such cases. We shall here

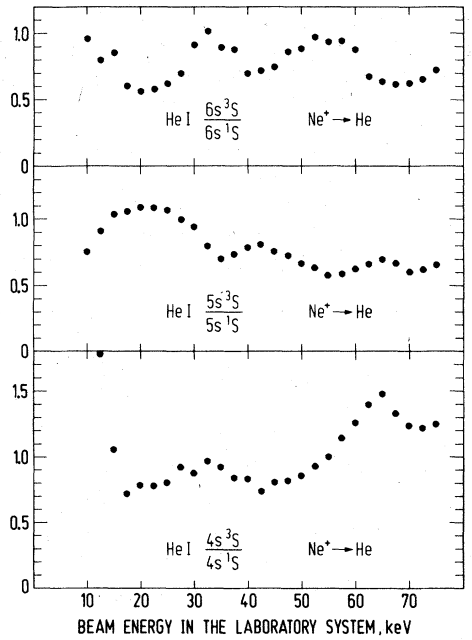

FIG. 6. HeI triplet-singlet cross-section ratios for Ne^+-He collisions.

mention one system which behaves slightly different from $(HeNe)^+$. In the Na^+-He collision a regular and quite pronounced oscillatory structure shows up in the HeI $4d\,^1D$ excitation cross section, whereas no structure is observed for the $4d\,^3D$ HeI level. This absence of structure for the triplet level can be explained from the spin conservation rule. Whereas $(HeNe)^+$ is a doublet, Na^+ and He have, in the initial channel, closed shells. Therefore, excitation of a triplet level in He must be accompanied by excitation of a triplet level in Na as well, because spin-orbit coupling can be assumed to be very small. This shifts the triplet potential energy curves to much higher energies than the corresponding singlets, so that HeI triplet excitation will proceed via several curve crossings (similarly to excitation of the HeII, NeII, and NeIII levels of this work, cf. Sec. III D), and this will wash out all structure. In agreement with this interpretation we find the triplet to singlet cross-section ratio much smaller in the Na^+-He collision than for Ne^+-He and He^+-Ne.

C. Superimposed oscillations

Both sets of HeI $4d\,^{1,3}D$ data (Fig. 3) show a characteristic superposition of two regular oscillations at the higher energies which is also observed for some of the other levels not reported here. The slow oscillations in the HeI $4d\,^{1,3}D$ data, as completed in thin line, behave in every respect as discussed above for HeI $3p\,^3P$, and the associated interference areas and ϕ_0 values are given in Table I. The superposition of a faster oscillation at the higher energies (above 6.4-keV center-of-mass energy) can be interpreted as the opening of a third strongly repulsive exit channel, No. 4 in Fig. 1, which crosses the entrance channel at the point C. The energy required to reach this crossing is the above mentioned threshold. The large interference area further supports this interpretation. Table II presents He and Ne energy levels[16] around the HeI $4d\,^{1,3}D$. The Ne levels have been displaced due to the difference in ionization potential so that a direct comparison is possible. Most likely NeI $4f$ is the term that mixes with HeI $4d$ to produce the slow oscillations in Fig. 3 because of its extreme proximity in energy. Also the HeI $4f$ is at 23.73 eV, but due to its high angular momentum it is strongly promoted[17] at close encounters. It approaches HeI $4d$ at a much smaller internuclear distance (point D in Fig. 1) than where the mixing of states 2 and 3 takes place, since the He subshell splitting is very small. As shown in Fig. 1, these are exactly the properties required by the hypothesized third exit channel, which makes HeI $4f\,^{1,3}F$ a very probable candidate. Its fast approach to HeI $4d$ and not NeI $4f$ further explains why two and not three interference patterns are observed. Such secondary oscillations with a threshold energy have not previously been reported. They give considerable information about the potential energy curves, not only by a new interference area, but also by the approximate location of the high-lying curve crossing with the entrance channel.

Many cross sections in the literature contain unaccounted for structure which should be analyzed for possible additional regular oscillations to extract the most information from the data. The He^+-Ne measurements of Muller and de Heer[15] are included on Fig. 3 and show very good agreement with our data. A similar double oscillation is found in the HeI $3p\,^3P$ cross section of Ref. 6 which is reproduced in Fig. 7. The Rosenthal analysis of the rapid oscillation extrapolates to a minimum in the cross section at $v^{-1}=5.5$ a.u. and a maximum at 0 a.u. Both these appear as gross features in Fig. 4, whereas the rise to a maximum at 11 a.u. is outside our energy region. The Ne potentials involved are those of the closely spaced NeI $3d$ levels.

TABLE II. He and Ne energy levels (Ref. 16) around HeI $4d\,^{1,3}D$.

Level	Energy (eV)
HeI $4d\,^3D$	23.729
$4d\,^1D$	23.729
$4f\,^3F$	23.730
$4f\,^1F$	23.730
NeI $4d\,[\frac{1}{2}]^\circ$	23.717 [a]
$4d\,[\frac{5}{2}]^\circ$	23.727 [a]
$4f\,[\frac{3}{2}]$	23.727 [a]
$4f\,[\frac{7}{2}]$	23.731 [a]

[a] (Level energy) + (ionization potential of He) − (ionization potential of Ne).

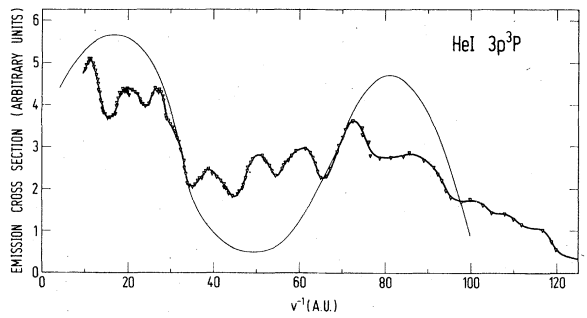

FIG. 7. Emission cross section for HeI $3p\,^3P$, from Ref. 6.

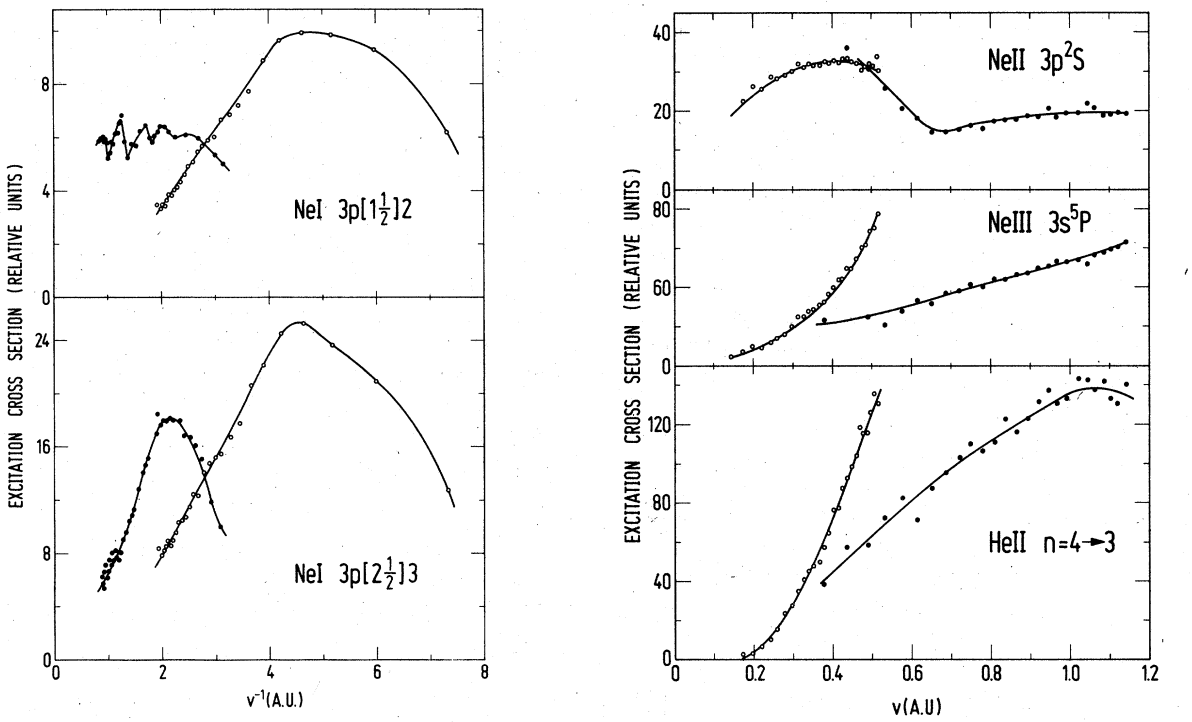

FIG. 8. Excitation cross sections for NeI $3p[1\frac{1}{2}]2$, NeI $3p[2\frac{1}{2}]3$, NeII $3p\,^2S$, NeIII $3s\,^5P$, and HeII $n=4\rightarrow n=3$. ●, He^+-Ne; ○, Ne^+-He.

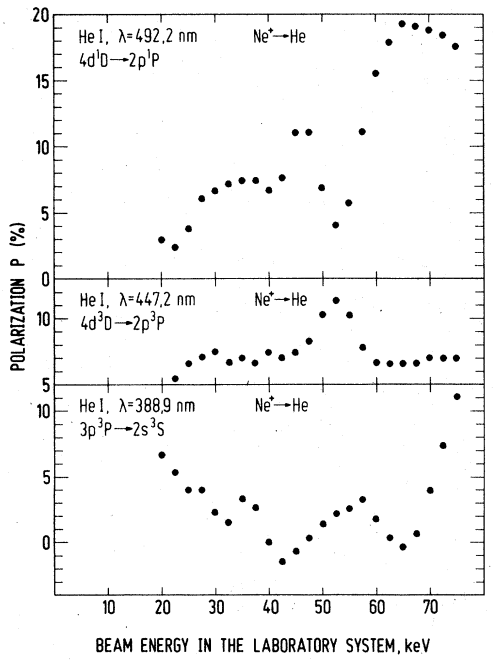

FIG. 9. Polarizations of HeI $4d\,^{1,3}D$ and $3p\,^3P$ in Ne^+-He collisions.

In their analysis Tolk *et al.*[6] only use the extrema at $v^{-1}>30$ a.u. However, also the high-energy oscillations, below 30 a.u., arise from the same interference area, but they are π out of phase. This phenomenon was predicted by Ankudinov *et al.*[3] to appear when, at some energy, the transition probability from the entrance channel (curve No. 1 in Fig. 1) to the upper exit channel (curve No. 3) is $\frac{1}{2}$, which in the present case seems to happen at $v^{-1}=32$ a.u. Such points of inflection will only appear at low collision energies where the transition probabilities at curve crossings are not vanishingly small.

D. He II and Ne cross sections, polarization

No or very little structure is observed in NeI, NeII, NeIII, and HeII excitation functions, see Fig. 8. The latter three types of states are produced only in close encounters and will interact with many different states so as to prevent regular oscillations as we observe them in e.g. Figs. 2–4. Neither potential curves[9,10] nor correlation diagrams[17] in combination with a two-state picture are applicable to such high excitations. The NeI $3p$ levels, on the other hand, are not highly ex-

cited, but they are well separated from all other levels and can therefore not produce an interference structure in the total cross section.

We note that for multi-electron processes of combined ionization and excitation (see e.g., the Ne III curve of Fig. 8) the cross sections are larger in that collision where the initial channel is more like the final one (i.e., Ne^+-He in this case).

Polarizations of He I line radiations show irregular changes as a function of the projectile velocity, and there is no correlation between polarizations of transitions from a singlet and the corresponding triplet. These features can be seen in Fig. 9. By comparing the curves of this figure with the corresponding total cross-section curves given in Figs. 3 and 4 it is furthermore seen that there is no relation between the variations in polarization (which reflects the relative excitation of magnetic substates of the upper level) and the variations in total level cross section. Earlier, structure in polarization effects in the collisions N^+, O^+, Na^+, Mg^+-Ne[18] and Na^+-Ne[19] was found to follow the structure of the total level cross sections. This appears not to be the case in general.

IV. CONCLUSIONS

The present measurements have pushed the limits of applicability of the Rosenthal model to higher energies where it was not *a priori* expected to work. The analysis of composite oscillatory structure in the excitation cross sections yields new information about the collision system and could, with sufficiently accurate data, be extended to several interfering states by Fourier analysis. Together with extensions to ion-surface scattering[20] this makes the Rosenthal model an increasingly powerful tool for interpreting atomic scattering data.

ACKNOWLEDGMENTS

The monochromators have been put at the authors' disposal by the Carlsberg Foundation and by the Danish National Research Foundation, which is gratefully acknowledged.

[1]T. Andersen, A. K. Nielsen, and K. J. Olsen, Phys. Rev. A 10, 2174 (1974).
[2]H. Rosenthal and H. M. Foley, Phys. Rev. Lett. 23, 1480 (1969); H. Rosenthal, Phys. Rev. A 4, 1030 (1971).
[3]V. A. Ankudinov, S. V. Bobashev, and V. I. Perel, Zh. Eksp. Teor. Fiz. 60, 906 (1971) [Sov. Phys. -JETP, 33, 490 (1971)]; S. V. Bobashev, in *Physics of Electronic and Atomic Collisions, Invited Lectures and Progress Reports of the Seventh International Conference on the Physics of Electronic and Atomic Collisions, Amsterdam, 1971* edited by L. M. Branscomb *et al.* (North-Holland, Amsterdam, 1972), p. 38.
[4]N. Andersen, K. Jensen, C. S. Newton, K. Pedersen, and E. Veje, Nucl. Instrum. Methods 90, 299 (1970).
[5]D. Coffey, D. C. Lorents, and F. T. Smith, Phys. Rev. 187, 201 (1969); M. Barat, J. C. Brenot, D. Dhuicq, J. Pommier, V. Sidis, R. E. Olson, E. J. Shipsey, and J. C. Browne, J. Phys. B 9, 269 (1976).
[6]N. H. Tolk, C. W. White, S. H. Dworetsky, and L. A. Farrow, Phys. Rev. Lett. 25, 1251 (1970).
[7]D. Hasselkamp, A. Scharmann, and K. -H. Schartner, in *Electronic and Atomic Collisions, Abstracts of the Papers of the Ninth International Conference on the Physics of Electronic and Atomic Collisions*, edited by J. S. Risley and R. Geballe (University of Washington Press, Seattle, 1975), p. 733.
[8]R. C. Isler, Phys. Rev. A 10, 2093 (1974).
[9]V. Sidis and H. Lefebvre-Brion, J. Phys. B 4, 1040 (1971).
[10]R. J. Blint, Phys. Rev. A 14, 971 (1976).
[11]K. Jensen and E. Veje, Nucl. Instrum. Methods 122 511 (1974).
[12]N. Andersen, K. Jensen, J. Jepsen, J. Melskens, and E. Veje, Appl, Opt. 13, 1965 (1974).
[13]N. Andersen, K. Jensen, J. Jepsen, J. Melskens, and E. Veje, Z. Phys. A 273, 1 (1975).
[14]W. L. Wiese, M. W. Smith, and B. M. Glennon, *Atomic Transition Probabilities*, NSRDS-NBS4 (U.S. GPO, Washington, D. C., 1966), Vol. 1.
[15]L. W. Muller and F. J. de Heer, Physica 48, 345 (1970).
[16]Charlotte E. Moore, *Atomic Energy Levels*, NBS Circ. No. 467 (U.S. GPO, Washington, D. C., 1949), Vol. 1.
[17]M. Barat and W. Lichten, Phys. Rev. A 6, 211 (1972).
[18]T. Andersen, A. K. Nielsen, and K. J. Olsen, Phys. Rev. Lett. 31, 739 (1973).
[19]N. H. Tolk, C. W. White, S. H. Neff, and W. Lichten, Phys. Rev. Lett. 31, 671 (1973); N. H. Tolk, J. C. Tully, C. W. White, J. Kraus, A. A. Monge, D. L. Simms, M. F. Robbins, S. H. Neff, and W. Lichten, Phys. Rev. A 13, 969 (1976).
[20]N. H. Tolk, J. C. Tully, J. Kraus, C. W. White, and S. H. Neff, Phys. Rev. Lett. 36, 747 (1976).